Engineering Nanospaces: OMS/Dendrimer Hybrids Possessing Controllable Chemistry and Porosity

Sukjoon Yoo,[†] Jonathan D. Lunn,[†] Sergio Gonzalez,[‡] Jennifer A. Ristich,[†] Eric E. Simanek,[‡] and Daniel F. Shantz*,[†]

Department of Chemistry, Texas A&M University, 3012 TAMU, College Station, Texas 77843-3012, and Department of Chemical Engineering, Texas A&M University, 3122 TAMU, College Station, Texas 77843-3122

Received September 13, 2005. Revised Manuscript Received April 12, 2006

The synthesis and characterization of melamine-based dendrimer/SBA-15-hybrids are reported. The current work demonstrates the ability to fabricate hybrid materials containing a high loading of organic moieties (∼30−35 wt %) that possess a well-defined structure. Numerous characterization methods including X-ray diffraction, electron microscopy, infrared spectroscopy, solid-state NMR spectroscopy, thermal gravimetric analysis, MALDI-MS, elemental analysis, and nitrogen porosimetry have been used to characterize the microstructure of the hybrids obtained. On the basis of thermal gravimetric analysis and elemental analysis, the average conversion between generations is between 70 and 75% and highly reproducible. MALDI-MS verifies that a significant fraction of the organic groups on the OMS surface possesses the desired structure, consistent with IR and NMR results. The porosity of the hybrid can be modified either by using dendrimers of different generations, using different linkers in the dendrimer structure, or by controlling dendrimer loading. Porosimetry measurements indicate that the effective pore size of the hybrid and the total pore volume of the material can be controlled independently of one another. Copper sequestration was used as a probe to demonstrate that the amines of the dendrimer are accessible and able to bind Cu(II). Given the ability to tune chemistry and porosity independently, the current work shows that these hybrid materials have potential uses in many areas including separations, sensing, and catalysis.

Introduction

Organic−inorganic hybrid materials have long attracted interest from the scientific and engineering communities.[1−4] These materials hold great promise in areas including sensing, separations, optics, and catalysis, given that they combine the features of both organic (e.g., chemical diversity) and inorganic (e.g., good mechanical/thermal properties) materials. Ordered mesoporous silicas (OMS)[5−12] have been studied extensively as supports for hybrid materials given that they possess an ordered pore structure containing uniformly sized pores, a variety of pore connectivities, and surfaces that can be easily functionalized using a wealth of previously developed silane chemistries.[13] These material properties facilitate analysis of the hybrid material by microscopy, powder X-ray diffraction (PXRD), and porosimetry and allow a relatively straightforward determination of how organic incorporation modifies the porosity and other properties of the parent OMS.

Numerous works have investigated incorporating organic functional groups into OMS.[13−18] These works have studied approaches including direct synthesis of hybrid materials, postsynthetic grafting, covalent versus noncovalent linkage, etc.[13−17] While most investigations have studied the grafting of simple silanes, more recent work has expanded to functional groups prepared by multistep reactions.[18−23] For

* Corresponding author. Phone: (979) 845-3492; fax: (979) 845-6446; e-mail: Shantz@che.tamu.edu.
[†] Department of Chemical Engineering.
[‡] Department of Chemistry.

(1) Loy, D. A.; Shea, K. J. *Chem. Rev.* **1995**, *95*, 1431−1442.
(2) Raman, N. K.; Anderson, M. T.; Brinker, C. J. *Chem. Mater.* **1996**, *8*, 1682−1701.
(3) Corriu, R. J. P. *Angew. Chem., Int. Ed.* **2000**, *39*, 1376−1398.
(4) Sanchez, C.; Lebeau, B.; Chaput, F.; Boilot, J. P. *Adv. Mater.* **2003**, *15*, 1969−1994.
(5) Beck, J. S.; Vartuli, J. C.; Roth, W. J.; Leonowicz, M. E.; Kresge, C. T.; Schmitt, K. D.; Chu, C. T. W.; Olson, D. H.; Sheppard, E. W.; McCullen, S. B.; Higgins, J. B.; Schlenker, J. L. *J. Am. Chem. Soc.* **1992**, *114*, 10834−10843.
(6) Kresge, C. T.; Leonowicz, M. E.; Roth, W. J.; Vartuli, J. C.; Beck, J. S. *Nature* **1992**, *359*, 710−712.
(7) Zhao, D. Y.; Feng, J. L.; Huo, Q. S.; Melosh, N.; Fredrickson, G. H.; Chmelka, B. F.; Stucky, G. D. *Science* **1998**, *279*, 548−552.
(8) Zhao, D. Y.; Huo, Q. S.; Feng, J. L.; Chmelka, B. F.; Stucky, G. D. *J. Am. Chem. Soc.* **1998**, *120*, 6024−6036.
(9) Ciesla, U.; Schüth, F. *Microporous Mesoporous Mater.* **1999**, *27*, 131−149.
(10) Davis, M. E. *Nature* **2002**, *417*, 813−821.
(11) Schüth, F.; Schmidt, W. *Adv. Mater.* **2002**, *14*, 629−638.
(12) Stein, A. *Adv. Mater.* **2003**, *15*, 763−775.
(13) Moller, K.; Bein, T. *Chem. Mater.* **1998**, *10*, 2950−2963.
(14) Burkett, S. L.; Sims, S. D.; Mann, S. *Chem. Commun.* **1996**, 1367−1368.
(15) Lim, M. H.; Blanford, C. F.; Stein, A. *J. Am. Chem. Soc.* **1997**, *119*, 4090−4091.
(16) Fowler, C. E.; Burkett, S. L.; Mann, S. *Chem. Commun.* **1997**, 1769−1770.
(17) Lim, M. H.; Stein, A. *Chem. Mater.* **1999**, *11*, 3285−3295.
(18) Alvaro, M.; Ferrer, B.; Garcia, H.; Hashimoto, S.; Hiratsuka, M.; Asahi, T.; Masuhara, H. *ChemPhysChem* **2004**, *5*, 1058−1062.
(19) Juvaste, H.; Iiskola, E. I.; Pakkanen, T. T. *J. Mol. Catal. A* **1999**, *150*, 1−9.
(20) Corriu, R. J. P.; Mehdi, A.; Reye, C.; Thieuleux, C.; Frenkel, A.; Gibaud, A. *New J. Chem.* **2004**, *28*, 156−160.
(21) McKittrick, M. W.; Jones, C. W. *Chem. Mater.* **2003**, *15*, 1132−1139.

10.1021/cm0520564 CCC: $33.50
Published on Web 06/01/2006

hybrids to achieve their full potential, it is necessary to be able to synthesize complex organic structures containing multiple functional groups and well-defined spatial arrangements directly on the mesoporous support. Such properties are of relevance in applications such as bifunctional catalysis and molecular recognition that require multiple functional groups or precise control over the spatial arrangement of functional groups. For emerging applications utilizing OMS such as drug delivery and sensing, it will be necessary to control particle size, chemical functionality, and porosity, ideally in an independent manner.[24]

The fabrication of OMS-hybrids with high densities of functional groups is particularly problematic. At high loading (>0.25 mmol/g), heterogeneity of sites is often observed,[25] and the formation of polymeric layers of the tethering agent is often problematic as well.[26] Recent work by the Jones lab has shown that surface patterning approaches can be used to circumvent this issue,[27,28] and work by the Katz lab has shown the potential of molecular imprinting to achieve higher (0.3−0.4 mmol/g) densities of homogeneous organic functional groups on amorphous silicas.[29−32] Another possible route to high functional group densities is the use of surface-tethered dendrimers. These highly uniform hyperbranched polymers[33−35] present unique opportunities given that increasing the dendrimer generation doubles the number of peripheral functional groups on the dendrimer. Further, dendrimers have shown promise in applications including catalysis, separations, and molecular recognition. Although physisorption of dendrimers into OMS has been successfully achieved,[36,37] covalent attachment is preferable in many applications.

The literature on dendrimers covalently attached to OMS is relatively sparse. Acosta et al. synthesized melamine-based dendrimers of various generations on SBA-15 mesoporous silica to bring the controllable chemistry and porosity to OMS.[38] Additionally, a collaboration between the Alper and the Al Sayari labs has produced three publications on PAMAM dendrimer-MCM-41-hybrids.[39−41] The current investigation, building off our preliminary report, expands the scope to other linkers in the dendrimers, as well as demonstrating that these materials can be used in applications such as metal sequestration. A thorough characterization study is presented using a battery of methods to determine the hybrid microstructure.

Experimental Procedures

Materials. Tetraethoxysilane (TEOS, ≥99%) was purchased from Fluka. Pluronic P123 ($EO_{20}PO_{70}EO_{20}$, MW = 5800) was obtained from BASF. Ethanol and toluene (ACS reagent grade) were purchased from EM Science. 3-(Aminopropyl)triethoxysilane (APTES, 99%), piperazine (P, 99%), 4,4′-trimethylenedipiperidine (TMDP, 97%), and *N*,*N*-diisopropylethylamine (DIPEA, 99%) were purchased from Aldrich. 4-(Aminomethyl)piperidine (AMP, ≥98%) was purchased from TCI America. Cyanuric chloride (CC, 99%) was purchased from ACROS. Tetrahydrofuran (THF), toluene, methanol, and dichloromethane (DCM) (all ACS solvent grade) were purchased from EMD. Copper(II)sulfate pentahydrate (cupric sulfate, ≥99%) was purchased from J. T. Baker. Ethylenediaminetetraacetic acid disodium salt (EDTA, ≥99%) was purchased from EM Science. Murexide (ammonium purpurate) was purchased from Acros. All chemicals were used as received.

Synthesis of Amine-Functionalized SBA-15. SBA-15 was synthesized using a method comparable to that reported previously.[8] 4.0 g of pluronic P123 was dissolved in 60 mL of 4 M HCl and 85 mL of deionized water by stirring for 5 h at room temperature. Then, 8.5 g of TEOS was added to that solution and stirred for 24 h at 35 °C. The mixture was then aged at 80 °C for 24 h under static conditions. The solid product was filtered, washed with copious quantities of deionized water, and air-dried overnight. The solid product was calcined to remove the pluronic used in the synthesis. The calcination procedure was as follows: the sample was heated from room temperature to 100 °C at a rate of 1 °C/min; held at 100 °C for 1 h; increased from 100 to 500 °C at a rate of 1 °C/min; and then held at 500 °C for 5 h. The amine-functionalized SBA-15 was prepared using postsynthetic grafting. An aliquot of APTES 16 μL (0.1 mmol), 80 μL (0.5 mmol), 160 μL (1.0 mmol), or 320 μL (2.0 mmol), depending on the desired amine loading, was added to 1 g of calcined SBA-15 in 100 mL of anhydrous toluene under nitrogen. This mixture was stirred overnight in a closed container at room temperature. The product was collected by filtration, washed with 1 L of deionized water, and air-dried.

Synthesis of Dendrimer-SBA-15 Composites. The synthesis of the composites is illustrated in Figure 1. A 0.3 M cyanuric chloride (CC) solution was prepared by adding 1.25 g of CC and 2.5 mL of diisopropylethylamine (DIPEA) (8 mmol) to 25 mL of tetrahydrofuran (THF). A 0.4 M 4-(aminomethyl)piperidine (AMP) solution was prepared by adding 1.25 g of AMP to 25 mL of THF. 0.4 M solutions were also prepared of piperazine (P) and 4,4′-trimethylenedipiperidine (TMDP). One gram of amine-functionalized SBA-15 was placed in a 30 mL vial, and 25 mL of the prepared CC solution was added. The vial was shaken for approximately 24 h at room temperature. The solution was filtered to remove the silica from the solution, and the silica was then rinsed with 50 mL

(22) McKittrick, M. W.; Jones, C. W. *J. Am. Chem. Soc.* **2004**, *126*, 3052−3053.
(23) Yu, K.; McKittrick, M. W.; Jones, C. W. *Organometallics* **2004**, *23*, 4089−4096.
(24) Huh, S.; Wiench, J. W.; Yoo, J.-C.; Pruski, M.; Lin, V. S. Y. *Chem. Mater.* **2003**, *15*, 4247−4256.
(25) Kanan, S. A.; Tze, W. T. Y.; Tripp, C. P. *Langmuir* **2002**, *18*, 6623−6627.
(26) Haller, I. *J. Am. Chem. Soc.* **1978**, *100*, 8050−8055.
(27) Jones, C. W.; McKittrick, M. W.; Nguyen, J. V.; Yu, K. *Top. Catal.* **2005**, *34*, 67−76.
(28) Hicks, J. C.; Jones, C. W. *Langmuir* **2006**, *22*, 2676−2681.
(29) Bass, J. D.; Anderson, S. L.; Katz, A. *Angew. Chem., Int. Ed.* **2003**, *42*, 5219−5222.
(30) Bass, J. D.; Katz, A. *Chem. Mater.* **2003**, *15*, 2757−2763.
(31) Bass, J. D.; Katz, A. *Chem. Mater.* **2006**, *18*, 1611−1620.
(32) Defreese, J. L.; Katz, A. *Microporous Mesoporous Mater.* **2006**, *89*, 25−32.
(33) Bosman, A. W.; Janssen, H. M.; Meijer, E. W. *Chem. Rev.* **1999**, *99*, 9, 1665−1688.
(34) Grayson, S. K.; Frechet, J. M. J. *Chem. Rev.* **2001**, *101*, 3819−3867.
(35) Tomalia, D. A.; Frechet, J. M. J. *J. Polym. Sci., Part A: Polym. Chem.* **2002**, *40*, 2719−2728.
(36) Díaz, I.; García, B.; Alsonso, B.; Casado, C. M.; Morán, M.; Losada, J.; Pérez-Pariente, J. *Chem. Mater.* **2003**, *15*, 1073−1079.
(37) Ottaviani, M. F.; Turro, N. J.; Jockbush, S.; Tomalia, D. A. *J. Phys. Chem. B* **2003**, *107*, 2046−2053.
(38) Acosta, E. J.; Carr, C. S.; Simanek, E. E.; Shantz, D. F. *Adv. Mater.* **2004**, *16*, 985−989.
(39) Reynhardt, J. P. K.; Yang, Y.; Sayari, A.; Alper, H. *Chem. Mater.* **2004**, *16*, 4095−4102.
(40) Reynhardt, J. P. K.; Yang, Y.; Sayari, A.; Alper, H. *Adv. Synth. Catal.* **2005**, *347*, 1379−1388.
(41) Reynhardt, J. P. K.; Yang, Y.; Sayari, A.; Alper, H. *Adv. Funct. Mater.* **2005**, *15*, 1641−1646.

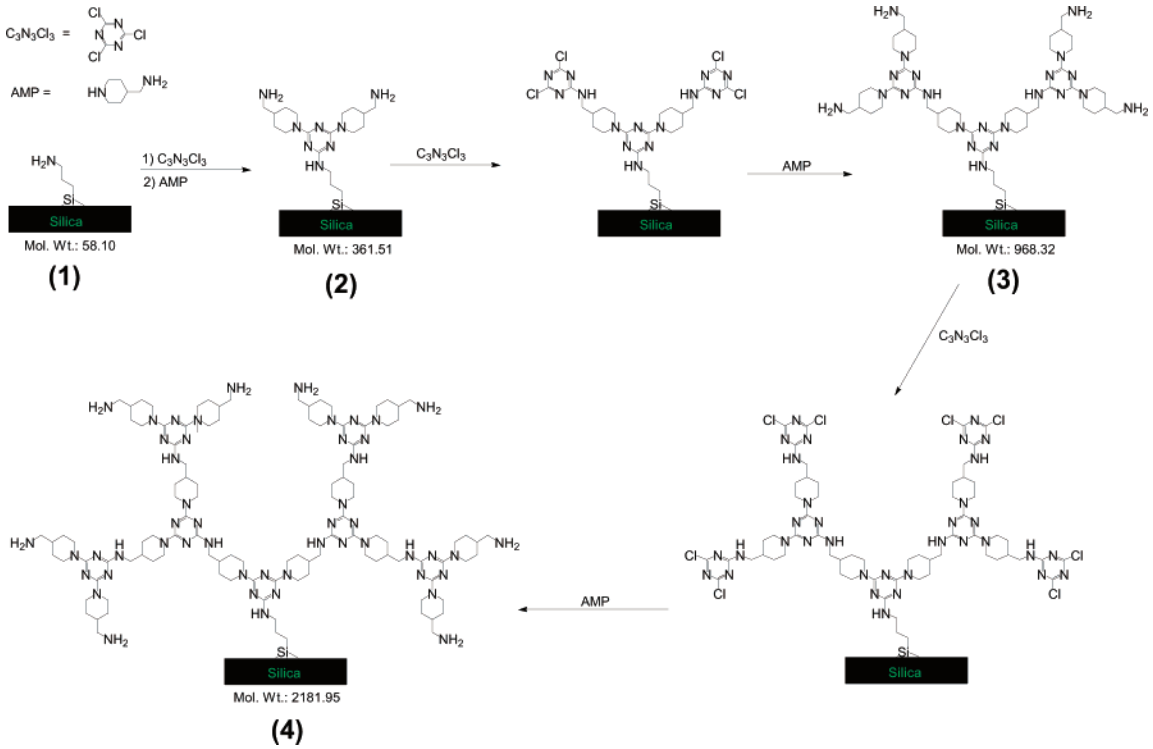

Figure 1. Iterative synthesis of melamine-based dendrimers of various generations on amine-functionalized SBA-15. Shown is the synthesis using 4-aminomethylpiperidine (AMP) as the linker molecule: (**1**) amine-functionalized SBA-15, (**2**) G1-AMP dendrimer, (**3**) G2-AMP dendrimer, and (**4**) G3-AMP dendrimer.

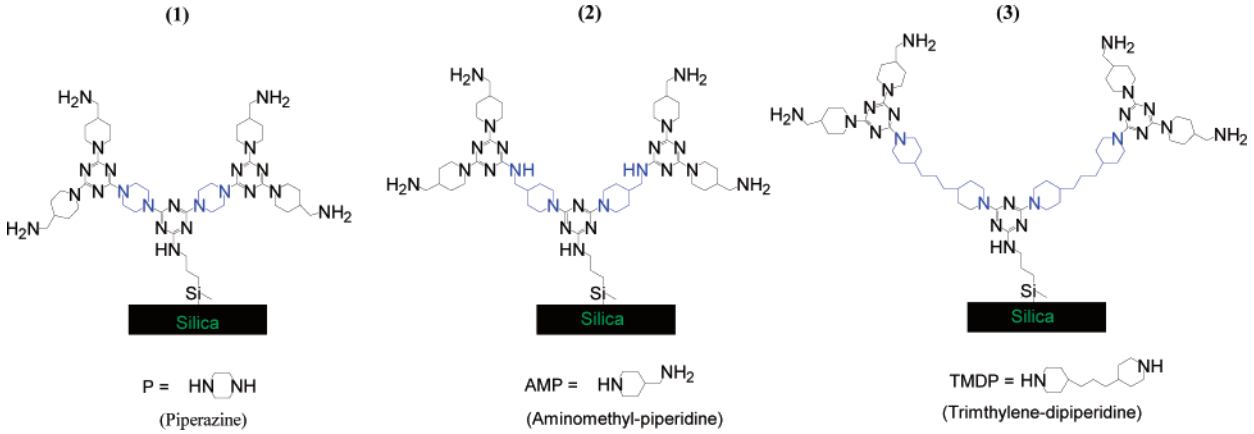

Figure 2. Synthesis of dendrimer-SBA15-hybrids using different linker molecules: (**1**) piperazine (P), (**2**) 4-(aminomethyl)piperidine (AMP), and (**3**) 4,4′-trimethylenedipiperidine (TMDP). Second-generation dendrimers are shown in all cases.

portions of methanol, dichloromethane, and THF sequentially. The silica was transferred back into a clean vial, 25 mL of the linker molecule solution was added, and the vial was again shaken for 24 h. The material was filtered and rinsed as described previously. The same procedure was followed to increase the dendrimer generation. So that every dendrimer had the same functionality on the outer periphery (primary amine), the final linker molecule used was AMP. Figure 2 shows a second-generation dendrimer for each linker molecule.

Analytical. Powder X-ray diffraction (PXRD) measurements were performed using a Bruker-AXS D8 powder diffractometer with Cu Kα radiation over a range of 0.8−5° 2θ. Peak intensities and 2θ values were determined using the Bruker program EVA. Transmission electron microscopy (TEM) was performed on a JEOL 2010 microscope with a lanthanum hexaboride filament and an excitation voltage of 200 kV. Infrared spectroscopy was performed on the G3 composites, amine-SBA-15, and SBA-15 using a Nexus 670 FT-IR spectrometer from Thermo Nicolet. ^{29}Si MAS and CP-MAS and ^{13}C CP-MAS were performed on a Bruker Avance operating at 79.49 and 100.61 MHz. All spectra were acquired using a 7 mm probe with ZrO_2 rotors and a spinning rate of 5080 Hz. ^{29}Si MAS spectra were acquired using a 2 μs 50° pulse, high-power proton decoupling, and a 90 s recycle delay. ^{29}Si{^{1}H} CP-MAS spectra were acquired with a 5 ms contact time, a ^{1}H 90° pulse length of 4 μs, and a 5 s recycle delay. ^{13}C{^{1}H} CP-MAS spectra were acquired with a 2.5 ms contact time, a ^{1}H 90° pulse length of 4 μs, and a 5 s recycle delay. Chemical shifts were referenced to tetramethylsilane. Thermal gravimetric analyses (TGA) were performed using a TG 209C Iris instrument from Netsch over a temperature range of 25−515 °C using oxygen as a carrier gas and temperature ramping rate of 5 °C min^{-1}. Mass spectra were acquired using MALDI-MS on an Applied Biosystems Voyager-DE STR Biospectrometry Workstation. Matrix-assisted laser desorption/ionization time-of-flight (MALDI-TOF) spectra were recorded in reflected ion mode with an Applied Biosystems Voyager DE-STR mass spectrometer (ABI, Framingham, MA). Positive ions were

generated by using a nitrogen laser pulse ($y = 337$ nm, 20 Hz) and accelerated under 25 kV using delayed extraction (190 ns) before entering the time-of-flight mass spectrometer. Laser strength was adjusted to provide minimal fragmentation and optimal signal-to-noise ratio. An average of 100 laser shots was used for each spectrum, and data were processed with the accompanying Voyager software package. The sample was prepared using the dry drop method with 2,4,6-trihydroxyacetophenone (THAP) as has been described previously.[38] The analysis solution, approximately 1 μM dendrimer and 10 mg/mL THAP solution in methanol, was spotted in 1 μL aliquots on top of a Teflon-coated plate. The samples were prepared for MS analysis by detaching the dendrons from the silica surface rather than dissolving the silica framework using HF. This detachment was performed by shaking approximately 20 mg of dendrimer/silica hybrid in 2 mL of a 1:1 concentrated HCl/methanol solution for 24 h. Elemental analysis (C, H, and N analysis) was performed by the Galbraith labs. Nitrogen-adsorption experiments were performed on a Micromeritics ASAP 2010 micropore system using approximately 0.1 g of sample. The samples were degassed under vacuum at room temperature for 2 h, then at 40 °C for 4 h, and then at 60 °C for 4 h before analysis. The micropore and mesopore volumes were determined using the α_s-method.[42,43] The mesoporous size distributions were calculated from the adsorption branch of the isotherm using the Barret−Joyner−Halenda (BJH) method[44] with a modified equation[45] for the statistical film thickness.

Copper(II) Sequestration. A total of 30 mg of the following samples was placed in vials: bare SBA-15; 0.5 mmol/g amine-SBA-15; and G1, G2, and G3 AMP-based composites (0.5 mmol/g amine loading). To these vials, 6.6 mL of 14.4 mM cupric sulfate in purified water (360.0 mg of cupric sulfate pentahydrate per 100 mL of water) was added. The mixtures were then shaken for 14 h. The resulting solutions were filtered, and 2 mL of each was titrated with 5.4 mM Na_2EDTA using murexide as the indicator (50.2 mg per 100 mL of purified water). Each solution was titrated twice, including the stock cupric sulfate solution.

Results

Powder X-ray diffraction was used to verify the hexagonal mesostructure of SBA-15 (Figure 3). The parent SBA-15-, amine-SBA-15-, and G1-hybrid materials show three well-defined peaks at 2θ values between 0.8 and 5° that can be indexed as the (100), (110), and (200) Bragg peaks, typical of hexagonal (*p*6*mm*) SBA-15.[7] The (100) peak is clearly observed as the dendrimer generation increases; however, the intensity of the (110) and (200) peaks decreases for the G2- and G3-hybrids. Subsequently, TEM was used to verify that SBA-15 retained its structural ordering (Supporting Information). The images show that the mesostructure is hexagonally ordered as expected.

Infrared spectroscopy was used to verify the presence of dendrimers in the materials. Figure 4 shows the spectra for SBA-15, amine-functionalized SBA-15, and the G3 composites of each linker molecule. The spectra show that the G3 composites are chemically different from SBA-15, the amine-SBA-15, and each other. The spectra exhibit the characteristic peaks for the primary, secondary, and tertiary carbon C−H bond stretches between 2800 and 3000 cm^{-1}. These peaks are not observed in the parent SBA-15 sample and are very weak for the amine-functionalized SBA-15. The intensity differences between the samples are due to the different linker molecules in the dendrimers. The dendrimer composites also show aromatic peaks between 1400 and 1600 cm^{-1}. The results are qualitative evidence for hybrid formation.

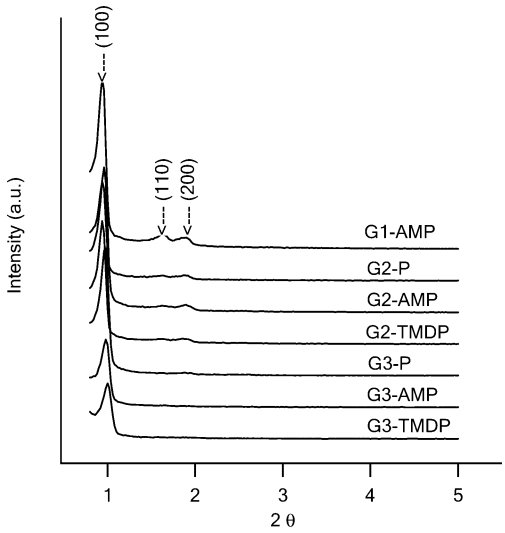

Figure 3. Powder X-ray diffraction patterns of the dendrimer-SBA15 composite materials.

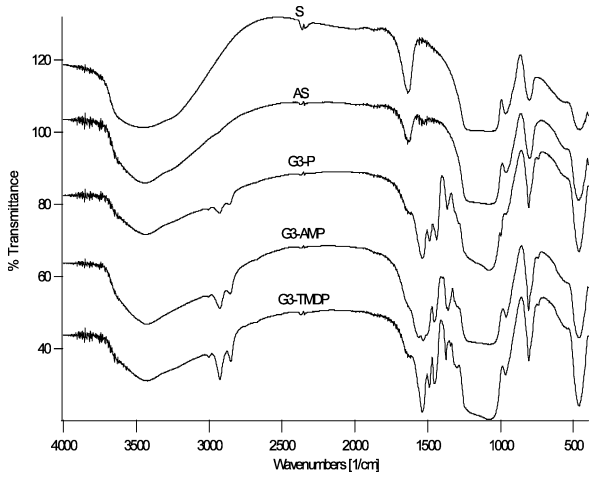

Figure 4. IR spectra of SBA-15 (S), 0.5 mmol/g NH_2−SBA-15 (AS), G3-P composite, G3-AMP composite, and G3-TMDP composite.

Further evidence for hybrid formation is obtained from solid-state NMR spectroscopy. Figure 5 shows the ^{29}Si MAS and $^{29}Si\{^1H\}$ CP-MAS spectra for the G3-AMP sample. Both spectra contain three broad sets of peaks between −90 and −110 ppm, consistent with Q^2, Q^3, and Q^4 silicon centers. The main differences between the spectra are the change in the relative intensities of the Q^3 and Q^4 lines and the resonance centered at approximately −67 ppm in the CP-MAS due to Si−C linkages, which is not observed in the one-pulse MAS spectra. The ^{29}Si NMR indicates that the silane is successfully grafted to the surface via the resonance observed at −67 ppm. The $^{13}C\{^1H\}$ CP-MAS (Figure 6) provides further evidence for the incorporation of the organic group. There is a line at 163 ppm due to the aromatic carbons,

(42) Gregg, S. J.; Sing, K. S. W. *Adsorption, Surface Area, and Porosity*; Academic Press: London, 1982.
(43) Rouquerol, F.; Roquerol, J.; Sing, K. *Adsorption by Powders and Porous Solids*; Academic: San Diego, 1999.
(44) Barrett, E. P.; Joyner, L. G.; Halenda, P. P. *J. Am. Chem. Soc.* **1951**, *73*, 373−380.
(45) Kruk, M.; Jaroniec, M.; Sayari, A. *Langmuir* **1997**, *13*, 6267−6273.

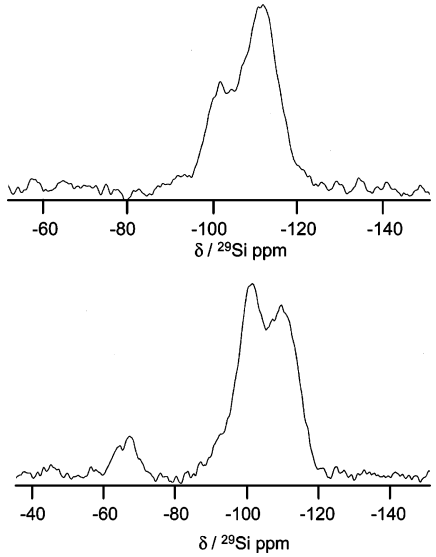

Figure 5. (Top) ^{29}Si MAS and (bottom) ^{29}Si{^{1}H} CP-MAS of the G3-AMP-hybrid.

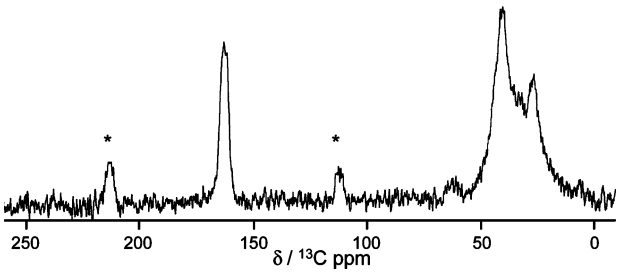

Figure 6. ^{13}C{^{1}H} CP-MAS spectrum of the G3-AMP-hybrid. Spinning sidebands are denoted with asterisks.

and the two resonances at 40 and 27 ppm are due to the aliphatic carbons on 4-aminomethylpiperidine. The carbons on the aminopropyl silane are obscured by these resonances, but a weak signal can be seen at approximately 6 ppm that is the methylene group attached to the silicon center. Also note that the aromatic carbons are quite rigid based on the spinning sidebands observed (marked with an asterisk). These results are consistent with the IR results. While it is not possible to rule out the presence of some reaction side products with NMR, the results qualitatively indicate the presence of dendrimers; this is studied further via MALDI-MS, as will be discussed next.

The organic content is quantified using thermal gravimetric analysis (TGA) and elemental analysis. The TGA results are summarized in Figure 7. The weight percent of organics increases by approximately 10% for each generation increase of AMP: 11wt % for G1, 20 wt % for G2, and 31 wt % for G3. On the basis of these values, the theoretical conversion at each stage is 31% (amine-SBA → G1), 75% (G1 → G2), and 83% (G2 → G3). A summary of the elemental analysis and TGA data is included in the Supporting Information. Using the elemental analysis data to estimate the conversions between G1 → G2 → G3 gives reasonable agreement with this. These values are consistent with previous work[38] but merit a few comments. First, the data shown are not corrected for the approximately 3.9% weight loss observed for the parent SBA-15, likely due to silanol condensation at elevated temperatures. This number was not subtracted from the subsequent samples as many of the silanol groups that

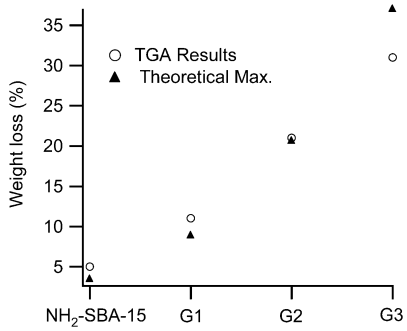

Figure 7. TGA results for the 0.5 mmol/g NH_2-SBA-15, G1-AMP composite, G2-AMP composite, and G3-AMP composite samples.

contribute to the weight loss react during the aminosilane functionalization step. However, not correcting the data results in the appearance that there is an excess of amine groups on the amine SBA-15 material. This in part contributes to the low conversion in going from the amine-SBA-15 material to the G1-hybrid. Two other factors that contribute to the low conversion in going from the amine SBA-15 material to the G1-hybrid are that some of the amines are simply not reactive and that some of the amines preferentially site in the micropores, inhibiting their subsequent reactivity. Three points appear consistent with this. First, the TGA data indicate that the amine grafting to the parent SBA-15 is essentially quantitative. Second, nitrogen adsorption of the parent material indicates a micropore volume of approximately 0.06 cm^3/g, whereas the amine-functionalized SBA-15 has no micropores that can be detected by α_s-analysis. Third, a sample of SBA-15 was calcined at 900 °C to collapse the micropores, and the G1 AMP-based composite was synthesized as described previously. TGA performed on this sample showed a yield of 45% of the G1 material, higher than the 35% yield for the sample with micropores (Supporting Information). That this value is still much lower than the other generations is likely due to the postsynthetic grafting method leading to inhomogeneity of the amine sites, rendering a fraction of them either inaccessible or unreactive. Elemental analysis (Supporting Information) is in good agreement with the TGA results.

TGA results for dendrimers made with the other two linkers also show clear trends. The increase in organic content per generation is approximately 8 wt % for P, 10 wt % for AMP, and 9 wt % for TMDP (Supporting Information). The result for piperazine is consistent with its lower molecular weight as compared to AMP. TMDP, however, does not behave as expected, as the organic content for a given dendrimer generation should be larger for this linker than with AMP or P. This result indicates that the TMDP is not as effective of a linker as AMP under the conditions used. This is likely due to side reactions (e.g., reactions between chloro groups on adjacent dendrimers) being more prevalent for the TMDP linkers. TGA results for samples with different initial amine loadings (Supporting Information) show that the amine loading can be increased or decreased without greatly influencing the overall yield of the G3 dendrimer growth: 24 % for 0.1 mmol/g and 20 % for 2.0 mmol/g. However, it is worth noting that the amount of amine deposited in the 1.0 mmol/g sample is the same as that for the 2.0 mmol/g sample, indicating an upper bound for

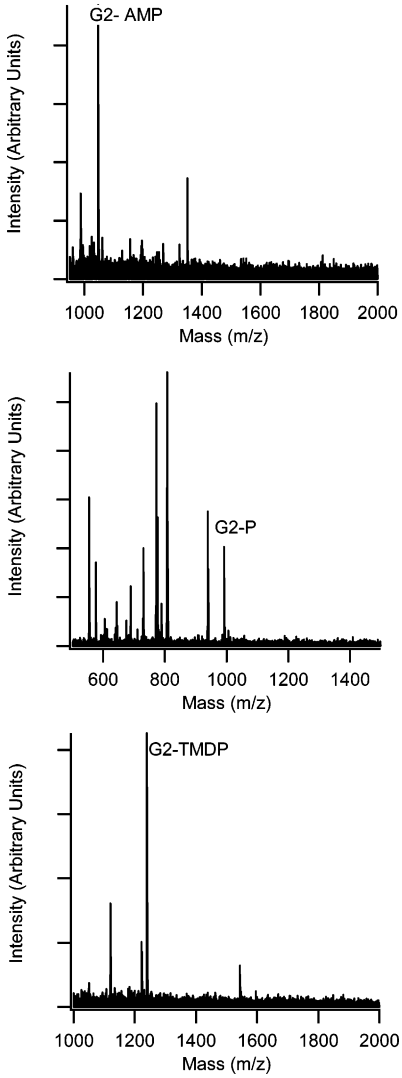

Figure 8. MALDI-MS (from top to bottom) for the G2-AMP-, G2-P-, and G2-TMDP-hybrids. Label in plot indicates position of the peak for the target dendrimer.

effective amine deposition. All of these materials were made in duplicate, and the TGA data are reproducible. Finally, it should be noted that the synthesis described previously has not been optimized to maximize the dendrimer yield on the silica substrate. The results show that this chemistry, which has been shown to proceed efficiently in solution,[46] can be extended to a solid support.

To further study the identity of the organic groups formed on the OMS surface, MALDI-MS was performed on the organic groups removed from the OMS. Figure 8 shows the MALDI-MS results for the samples G2-AMP, G2-P, and G2-TMDP. The exact masses for the G2-AMP, G2-P, and G2-TMDP dendrons are 1024, 990, and 1238, respectively. Significant peaks representing each of these masses (M + H) are prevalent in the mass spectra. These results are consistent with the NMR, TGA, and elemental analysis that indicate that the bulk of the groups on the OMS surface are in fact the desired dendrimer moieties. While the conversion/yield at each stage is not quantitative, the mass spectrometry is the strongest evidence that the desired dendrimer groups are formed on the OMS surface.

(46) Zhang, W.; Simanek, E. E. *Org. Lett.* **2000**, *2*, 843−845.

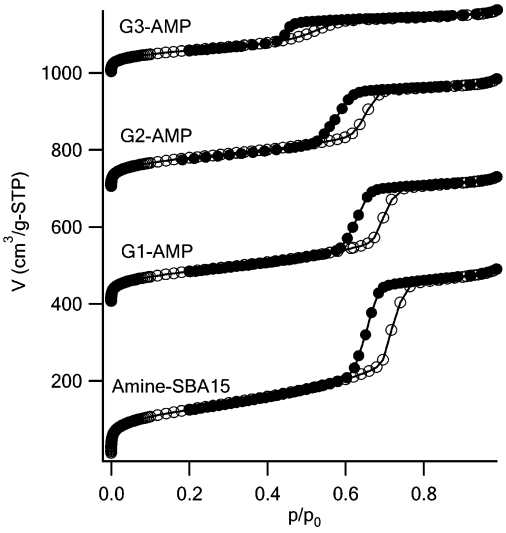

Figure 9. Adsorption isotherms for the dendrimer-SBA-15 composite materials: effect of the dendrimer generation. Adsorption branches are represented by open circles, desorption branches by solid circles. The isotherms are shifted 400, 700, and 1000 cm^3/g STP for G1-, G2-, and G3-AMP, respectively.

Nitrogen Adsorption. Nitrogen adsorption was used to quantify the change in porosity of the OMS substrate. The porosity of the dendrimer-SBA15 composite materials can be systematically controlled by increasing the dendrimer generation, dendrimer loading, and using three different linker molecules (P, AMP, and TMDP). Figure 9 shows the nitrogen-adsorption isotherms for the first three generations of the AMP-based dendrimer composite. As shown in Figure 9, the relative pressure at which capillary condensation occurs shifts systematically to lower relative pressures as the dendrimer generation increases. This is consistent with the BJH analysis, which shows a decrease of the effective mesopore diameter from 7.5, to 6.7, to 5.2 nm for G1-AMP, G2-AMP, and G3-AMP, respectively. Given the large organic content of these samples and the lack of a suitable reference material, it should be emphasized that the pore sizes derived from the BJH analysis are subject to some error. That said, clear trends are observed consistent with an increase of organic content in the SBA-15 mesopores and the TGA, elemental analysis, and mass spectrometry results. The pore volume also systematically decreases from 0.59, to 0.41, to 0.20 $cm^3\ g^1$ as the dendrimer generation increases from G1-AMP, to G2-AMP, to G3-AMP, respectively. These values are comparable to previous work.[38] These results indicate that a considerable fraction of dendrimers is formed in the mesopores and that the porosity can be controlled by changing the dendrimer generation.

The porosity of the composite materials can also be controlled using different linker molecules in the dendrimer synthesis. Figure 2 shows each linker molecule and the second-generation dendrimer. The linker molecules trend in size as P < AMP < TMDP. Figure 10 shows the nitrogen-adsorption isotherms for the different G1−G3-hybrids with the different linkers. A shift of the hysteresis loop to a lower pressure is observed as the size of linker molecule increases. Table 1 summarizes the adsorption results for the different samples investigated. The effective mesopore diameter, surface area, and volume adsorbed decrease as the dendrimer

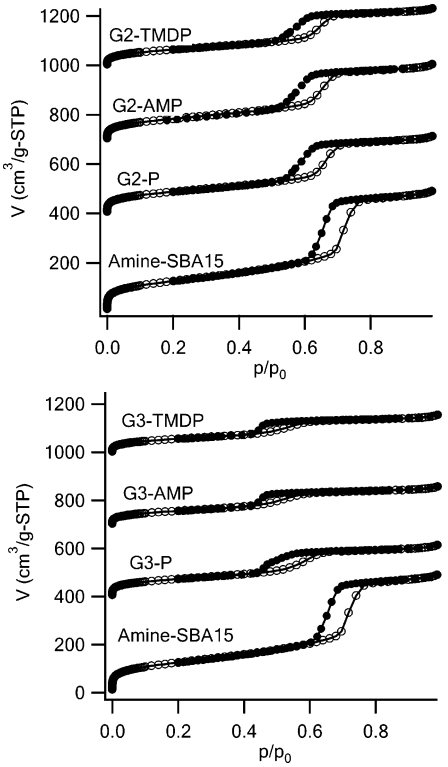

Figure 10. Adsorption isotherms for the dendrimer-SBA-15 composite materials: effect of the linker molecule. (Top) G2-hybrids and (bottom) G3-hybrids. Adsorption branches are represented by open circles, desorption branches by solid circles. The isotherms are shifted 400, 700, and 1000 cm^3/g STP for P, AMP, and TMDP in the second and third generation, respectively.

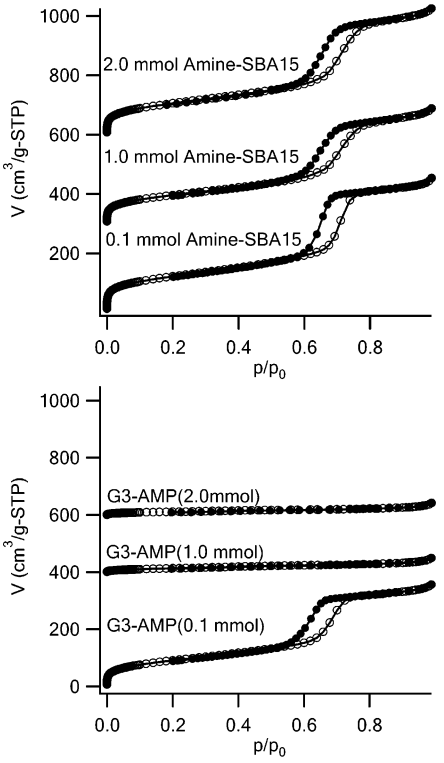

Figure 11. Adsorption isotherms for the dendrimer-SBA-15 composite materials: effect of the initial amine loading. Adsorption branches are represented by unfilled circles, desorption branches by solid circles. The isotherms are shifted 300 and 600 cm^3/g STP for 1.0 mmol/g NH_2-SBA15 and 2.0 mmol/g NH_2-SBA15, respectively. The isotherms are shifted 400 and 600 cm^3/g STP for G3-AMP (1.0 mmol/g) and G3-AMP (2.0 mmol/g), respectively.

Table 1. Adsorption Data Summary for the Dendrimer-SBA-15-Hybrids

sample	S(BET) [m^2/g]	$S(\alpha_s)$ [m^2/g]	V_{meso} [cm^3/g]	D_p(BJH) [nm]
0.5 mmol of amine	438	435	0.70	7.9
G2 P	302	307	0.43	7.0
G3 P	254	256	0.27	5.9
G1 AMP	429	414	0.59	7.5
G2 AMP	286	297	0.41	6.7
G3 AMP	193	205	0.20	5.2
G2 TMDP	220	228	0.31	6.7
G3 TMDP	194	200	0.19	5.2

size increases by changing the linker molecule from P to AMP. But both AMP and TMDP show similar values in the pore size, surface area, and volume adsorbed in each generation. These similar values reflect the lower yields in the TMDP dendrimers as compared to the AMP system, consistent with the TGA data as stated previously. The results show that using dendrimers with different linker molecules is also a route to controlling the hybrid porosity.

The initial amine loading was varied from 0.1 to 2.0 mmol per gram of SBA-15 to increase the organic content of the composites. Figure 11 shows the nitrogen-adsorption isotherms for the various initial amine loadings and its third-generation AMP dendrimer. The isotherms indicate that the mesopores of SBA15 are completely filled by the dendrimer for the samples with high initial amine loading. The G3-AMP with higher initial amine loadings (1.0 and 2.0 mmol) shows a dramatic decrease in both the surface area and the volume adsorbed values as compared to the samples with lower initial amine loadings (0.1 and 0.5 mmol). The samples prepared with high initial amine loadings (1.0 and 2.0 mmol) containing the G3-dendrimers are essentially nonporous, in contrast to the samples with lower initial amine loadings (0.45 and 0.20 cm^3/g for 0.1 and 0.5 mmol, respectively). Also noteworthy is that the 1 and 2 mmol/g amine-loaded samples appear very similar, consistent with the TGA data, indicating that they have the same amine content. This is also consistent with the TGA data that shows a substantial difference in organic content between the third-generation composites grown on SBA-15 with high initial amine loadings, 38 wt %, as compared with SBA-15 with the lowest amine loading, 17 wt %. This result shows that the effective porosity can be modulated for a given dendrimer chemistry and oxide substrate by adjusting the dendrimer loading.

The results demonstrate that OMS/dendrimer hybrids can be formed by the stepwise synthesis of melamine-based dendrimers grown directly off the mesopore surface. The adsorption results indicate that the porosity of hybrids can be engineered by adjusting dendrimer generation, linker molecule, and organic loading in a controllable way. The trends observed in the nitrogen-adsorption data support this as the effective pore diameters, volumes, and surface areas decrease with increasing dendrimer generation for a fixed linker, increasing the linker size for a fixed dendrimer generation, or increasing the amine loading on the surface. The one exception to this is that AMP and TMDP show similar pore volumes and diameters even though TMDP is larger. This is consistent with TGA and elemental analysis results that show that the TMDP is not as reactive/effective of a linker as AMP. Also, the high initial amine loading leads

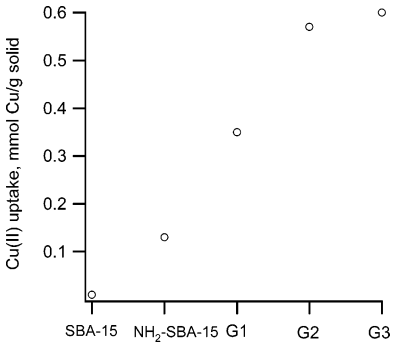

Figure 12. Copper(II) sequestration results for SBA-15, 0.5 mmol/g NH_2-SBA-15, G1-AMP composite, G2-AMP composite, and G3-AMP composite.

to a dramatic decrease in surface area and pore volume, which correlates with the increase of organic content determined by TGA.

Copper(II) Sequestration. Copper(II) sequestration was used to demonstrate the accessibility of the amines and the increased separation potential of higher generation dendrimer composites. Evidence for recognition of Cu(II) by melamine-based dendrimers in solution has already been reported by Zhang and co-workers.[47] Here, it is demonstrated that this binding is still efficient when the dendrimers are tethered to a solid support. A 4-fold excess of cupric sulfate and a significant period of exposure (14 h) were used to determine the maximum sequestering potential of the dendrimer composites. The results of this experiment are shown in Figure 12. Comparing Figure 12 with Figure 7, which shows the organic content for these same samples, demonstrates the positive correlation between dendrimer size and maximum amount of copper that can be sequestered. As expected, SBA-15 proved to be a very poor copper scavenger, taking up a negligible amount of copper, 0.01 mmol/g. This result indicates that the copper uptake observed in the hybrids is not an artifact of copper binding to silanol groups. The amine-SBA-15 and dendrimer composites were able to sequester significant amounts of copper: 0.13, 0.35, 0.57, and 0.60 mmol/g for amine-SBA-15 and the G1, G2, and G3 AMP-based composites, respectively. Ongoing work is exploring the coordination/complexation of the copper to the dendrimer. One possible explanation for the plateau in copper uptake in going from the G2 to the G3 dendrimer is that for the G3 system, the copper can only complex on the outer surface (i.e., to peripheral amines). If that were the case, based on TGA data, it can be estimated there are approximately 0.58 mmol/g solid of periphery amines on the G3 dendrimer, in reasonable agreement with the uptake data. Ottaviani and co-workers studied copper binding in PAMAM dendrimers and concluded that it is possible for copper to bind amines in the dendrimer interior.[48,49] The data for the G1 and G2 samples would seem consistent with their work.

(47) Zhang, W.; Simanek, E. E. *Tetrahedron Lett.* **2001**, *42*, 5355−5357.

Conclusion

Dendrimer-SBA-15-hybrids are synthesized and characterized using several analytical techniques. The hybrid porosity can be systematically altered by varying the dendrimer generation, the linker molecule, and the surface amine loading. Given the accessibility demonstrated by Cu(II) sequestration, the materials have accessible functional groups that can be used for catalysis, separations, molecular recognition, or as scaffolds to build more complex structures. Ongoing work is optimizing the synthesis conditions for higher dendrimer yields, and our results suggest that the presence of micropores had a deleterious effect on dendrimer yield.

Acknowledgment. This work was supported by NSF Grant CTS-0329386. The authors also acknowledge the Microscopy and Imaging Center (MIC) at Texas A&M for access to the TEM facilities and the Chemistry Department (TAMU) for access to the powder X-ray diffraction instruments and the Laboratory for Biological Mass Spectrometry.

Supporting Information Available: Elemental analysis of selected samples, TGA data for all samples studied in tabulated form, tabulated adsorption data for samples with different initial amine loadings, and TGA data for amine and G1-hybrid using SBA-15 with and without micropores. This material is available free of charge via the Internet at http://pubs.acs.org.

CM0520564

(48) Ottaviani, M. F.; Bossmann, S.; Turro, N. J.; Tomalia, D. A. *J. Am. Chem. Soc.* **1994**, *116*, 661−671.

(49) Ottaviani, M. F.; Montalti, F.; Turro, N. J.; Tomalia, D. A. *J. Phys. Chem. B* **1997**, *101*, 158−166.